2015 IEEE International Conference on Robotics and Automation (ICRA)
Washington State Convention Center
Seattle, Washington, May 26-30, 2015

Touch-down angle control for spring-mass walking

Hamid Reza Vejdani[1], Albert Wu[2], Hartmut Geyer[2], and Jonathan W Hurst[1]

***Abstract*— In this paper we propose the fastest converging control policy (also known as deadbeat control) for walking with the bipedal spring-mass model, which serves as an abstraction of a robot on compliant legs. To fully leverage the passive dynamics of the system, the touchdown angle of the swing-leg is assigned as the only control input of the system. We show that two steps (or one stride) are necessary and sufficient to converge to target walking gaits.**

We first analyze the dynamics of the system to identify the limit cycles as well as the limitations of the control authority within the definition of walking. Then, we present the two-step deadbeat control policy that guarantees stability with the fastest possible convergence rate for the system. For each equilibrium gait, the basin of attraction in which this two-step control exists is a measure of the robustness of the system. The simulation results show that human-like walking gaits (double hump ground reaction force profile) have relatively large basins of attraction. Finally, we extend the policy to various energy levels to accommodate walking on uneven ground that has height changes. We show in simulation that the system indeed rejects various disturbances and converges to the desired equilibrium gait in two steps.

I. Introduction

We use the bipedal spring-mass model as the template for control and design of walking and running robots [1], [2] and in this paper we derive the control strategy from the dynamics of the model. The bipedal spring-mass model represents the system as a lumped mass attached to two massless elastic legs (Figure 1). Inspired by human locomotion, it captures key characteristics from the dynamics of human walking [3], [4] including the shape of the ground reaction force profile and the center of mass (CoM) oscillation. This model is a natural extension of the spring loaded inverted pendulum model (SLIP) which has been widely used in literature for modeling and controlling running systems [5], [6], [7], [8], [9].

Using the bipedal spring-mass model, researchers have identified limit cycles for walking, analyzed the stability of these gaits, and investigated the transitions between them. They have applied the resulting insights towards robot control and understanding animal locomotion. However, these existing techniques do not take full advantage of the behavior that can be theoretically achieved through manipulating the landing angle by investigating the whole state space in finding the appropriate angle of attack at each step.

[1]Hamid Reza Vejdani and Jonathan W Hurst are with the school of Mechanical, Industrial and Manufacturing Engineering at Oregon State University, Oregon, USA. e-mail: hamidrvn@gmail.com; jonathan.hurst@oregonstate.edu

[2]Albert Wu and Hartmut Geyer are with the Robotics Institute, Carnegie Mellon University, PA, USA e-mail: albertwu87@gmail.com; hgeyer@cs.cmu.edu

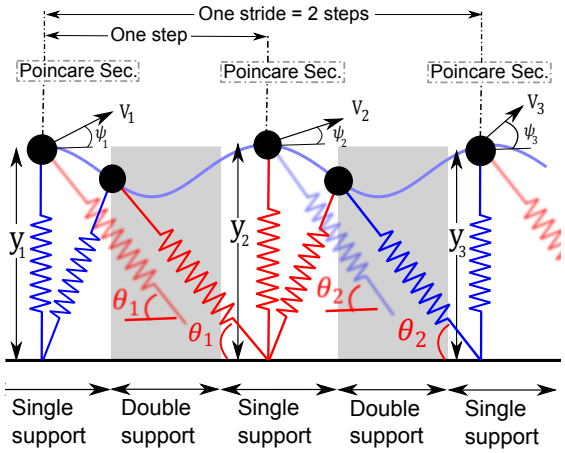

Fig. 1. The bipedal spring-mass model with single support phase and double support phase. The Poincare section is defined during the single support phase where the stance leg has vertical orientation. The states of the system at the Poincare section are y and ψ. One step is defined from one Poincare section to the next Poincare section and the touchdown angle of the swing leg is shown by θ_1 in the first step and θ_2 in the second step.

Rummel et al [10] investigated the role of the leg parameters of the bipedal spring-mass model for robustness and efficiency. Using a constant angle of attack control policy, in their analysis of the system they found five types of equilibrium gaits with different basins of attraction and local convergence properties.

Through defining the concepts of finite stability and viability, Salazar et al [11] analyzed the model under constant angle of attack policies to demonstrate stability of certain gaits and the ability to transition between gaits across many steps.

The spring-mass model has also been used as a template for controlling full body model of robots [12], and Garofalo et al [13] applied this model to control a fully actuated robot in simulation.

Andrada et al. [14] showed that keeping the angle between the two legs constant leads to robust and finite stable ground running gaits, which may explain how quails walk; while Maus et al [15] extended the model to 3D and walking in a circle to potentially explain how blindfolded or disoriented people walk.

In this paper, we systematically map out the dynamics of the bipedal spring-mass model as state to state transitions using leg placement as a control input. From this mapping, we identify deadbeat control that converges to target gaits in the minimum number of steps, and the control is defined over explicit regions of attraction. First, by defining Poincare

sections and tabulating the transitions in an appropriate state space, we identify a workspace that captures all possible walking behaviors allowed by the model. Within this workspace, any state has a non-zero region of attraction from which the state can be reached in two steps. Specifically, we deadbeat stabilize the equilibrium gaits with a two-step policy in their regions of attraction, thus achieving the fastest possible convergence. The size of the region of attraction and the relative location of the equilibrium state describes the robustness of each gait. Finally, while the workspace is defined for a constant system energy, we extend the control across different energy levels to demonstrate robust walking on simulated uneven ground.

II. DYNAMICS OF THE BIPEDAL SPRING-MASS MODEL

In the bipedal spring-mass model two massless elastic legs are attached to a point mass body [3], [4], [11], and when only one leg is on the ground, the system is equivalent to a spring loaded inverted pendulum (Figure 1). The springs store and return energy, rendering the system theoretically conservative with no energy losses. While in this model there are no impact losses like in other hybrid walking models [16], [17], [18], [19], [20], this model still has hybrid dynamics due to the distinct single support and double support phases in which respectively only one or both legs are on the ground. In each phase, the dynamics are as follows:

single support:

$$\begin{Bmatrix} \ddot{x} \\ \ddot{y} \end{Bmatrix} = \begin{Bmatrix} \frac{F_1(x-x_{t1})}{m.l_1} \\ \frac{F_1(y-y_{t1})}{m.l_1} - g \end{Bmatrix} \tag{1}$$

double support:

$$\begin{Bmatrix} \ddot{x} \\ \ddot{y} \end{Bmatrix} = \begin{Bmatrix} \frac{F_1(x-x_{t1})}{m.l_1} + \frac{F_2(x-x_{t2})}{m.l_2} \\ \frac{F_1(y-y_{t1})}{m.l_1} + \frac{F_2(y-y_{t2})}{m.l_2} - g \end{Bmatrix} \tag{2}$$

where the spring compression force F_i and length l_i of each leg are given by

$$F_i = k(l_0 - l_i) \geq 0 \quad i = 1, 2 \tag{3}$$

$$l_i = \sqrt{(x - x_{ti})^2 + (y - y_{ti})^2} \quad i = 1, 2 \tag{4}$$

In these equations, $[x,\ y]$ are the coordinates of the center of mass (CoM), $[x_{ti},\ y_{ti}]$ are the coordinates of each toe, and the parameters m, k, l_0, and g are respectively the mass, spring stiffness, rest length, and gravitational acceleration.

Single support transitions to double support when the CoM has negative vertical velocity and the condition $y = l_0 \sin(\theta)$ is fulfilled where θ is the touchdown angle of the swing leg and we use this value, which parameterizes leg placement, as the single control input of the system. Double support transitions to single support when the spring deflection $l_0 - l_i$ of one leg returns to zero.

A. State space and discrete dynamics

The state space of the bipedal spring-mass model for walking is the set of all the independent states that the system can take in the process of walking. The state space of a system can be parameterized by any set of values that are sufficient to resolve the dynamics, and the representation can be further simplified by defining a Poincare section to convert the system into a series of discrete states [21], [22].

Similar to [10], [23], we define the Poincare section at the vertical leg orientation (VLO) in single support (illustrated in Figure 1). At this condition, the system dynamics and subsequent states can be computed from the height y_n of the CoM and the orientation ψ_n of the velocity vector of the CoM, assuming a control input θ_n for the landing angle of the free leg (subscript $_n$ is used to denote the indexing of the now-discretized system). This holds true because the system has constant energy E, so magnitude $|v_n|$ of the velocity is known given the height y_n and are related through

$$E = \frac{k(l_0 - y_n)^2}{2} + mgy_n + \frac{mv_n^2}{2}. \tag{5}$$

Therefore, we define the discrete states at the Poincare sections as

$$\boldsymbol{X_n} = \begin{Bmatrix} y_n \\ \psi_n \end{Bmatrix} \tag{6}$$

and express the state-to-state transitions as the following discrete mapping:

$$\boldsymbol{X_{n+1}} = A(\boldsymbol{X_n}, \theta_n), \tag{7}$$

since $\boldsymbol{X_n}$ and θ_n provide sufficient information to integrate the equations of motion between Poincare sections.

Using a feedback controller for the control input ($\theta_n = H(\boldsymbol{X_n})$) and substituting it to the dynamics of the system, we will obtain the return map ($f : \chi \to \chi$)

$$\boldsymbol{X_{n+1}} = A(\boldsymbol{X_n}, H(\boldsymbol{X_n})) = f(\boldsymbol{X_n}), \tag{8}$$

where manifold χ contains all possible Poincare states $\boldsymbol{X_n}$.

III. WORKSPACE OF WALKING AND EQUILIBRIUM GAITS

We start by defining the workspace as all the VLO states that the model can encounter while continuously walking. To find the workspace, we look for two different sets in the state space: the start states, which are all the initial conditions $\boldsymbol{X_n}$ from which a subsequent Poincare section ($\boldsymbol{X_{n+1}}$) can be successfully reached for at least one value of θ_n; and the reachable states, which are all the subsequent states $\boldsymbol{X_{n+1}}$. Here, we take "successfully reach" to mean entering the next Poincare section without falling or entering the flight phase. In the $[y,\ \psi]$ plane of states, these two sets are reflections of each other across the $\psi = 0$ axis, since any trajectory from $\boldsymbol{X_n}$ to $\boldsymbol{X_{n+1}}$ is also a legitimate trajectory from $\boldsymbol{X_{n+1}}$ to $\boldsymbol{X_n}$ if played in reverse (i.e, Figure 1 from right to left), which effectively changes the sign of ψ. By definition, the workspace is simply the intersection of the start states and the reachable states.

To find the aforementioned sets, we mesh the $[y,\ \psi]$ plane of possible VLO states (as was mentioned in [11]) into grids

of size ($\delta y = 2.5mm, \delta\psi = 1°$), scan over touchdown angles with an increment of $\delta\theta = 0.1°$, and integrate the dynamics from each set of initial conditions. Equilibrium points $\boldsymbol{X_n}$, corresponding to a periodic limit cycle repeated between sequential single support phases, exist wherever

$$\boldsymbol{X^*} = A(\boldsymbol{X^*}, \theta^*) \tag{9}$$

for some landing angle θ^*. Similar to [10], we use Newton-Raphson iteration to interpolate equilibrium points between sampled grid points.

To accomplish the simulations, the model was implemented in Matlab (R2012a, Mathworks Inc., Natick, MA, USA) and the following properties for the robot (table I) were assumed. To solve the differential equations, ode45 (a Matlab function that solves ordinary differential equations based on the explicit 4/5-order Runge-Kutta method) was used with relative and absolute tolerances equal to 1e-11.

TABLE I

PROPERTIES OF THE SPRING-MASS ROBOT

Parameter	Description	Value
m	robot mass	$58.0kg$
k	leg spring stiffness	$12000\frac{N}{m}$
l_0	initial leg length	$0.85m$

A. Workspace in one energy level

To find the workspace of the system, first all the states that can start and complete at least one walking gait are found (start states). After that, we find the reachable states that can be reached at the end of walking gaits. The intersection of these two sets is the workspace of the system and includes all the states that come from a walking gait and can continue the process of walking.

In Figure 2 the aforementioned sets are shown in different colors (green for start states, blue for reachable states and gray to represent the workspace). The workspace has an elliptical shape and represents all the states that are useful for sequential walking. The equilibrium points are distinguished separately by the red color. There are both symmetric and asymmetric equilibrium points in the state space in one energy level. The force profiles for the various types of equilibrium gaits are shown along with their center of mass trajectories from grounded running type of gait to double hump human walking behavior.

If due to some disturbances the states of the system are located outside of the workspace, the system can not continue walking. Therefore, the control authority of the bipedal spring-mass model with the touchdown angle control input is limited to the size of this region.

1) Characterization of the equilibrium gaits: The equilibrium gaits in one energy level are shown in Figure 2 as a continuum changing behavior of the system. The force profiles of symmetric gaits evolve from a single hump in the middle of the workspace to a flat shape as it goes to the right and gradually to a double hump (like what we observe from typical human walking [3]) and finally at the far right side of the workspace it looks like hopping with both legs. The shapes of the force profiles for the equilibrium gaits are consistent with the results in [10]. The different behavior of equilibrium gaits provides various choices for limit cycle walking gaits and can also be useful to explain different locomotion gaits in nature. For example, the schematic force profile of chimpanzee walking gait and the corresponding CoM trajectory of that, is located in the middle of the elliptical [24] while the behavior of human walking gait can be explained by another gait in the right side of the workspace [3], while for grounded running birds like quail the equilibrium gaits are in the left side of the ellipse [14]. We speculate that the differences between the types of walking gaits that we observe from different animals depend on the morphology and mechanism of their legs and each gait is optimized for its mechanism.

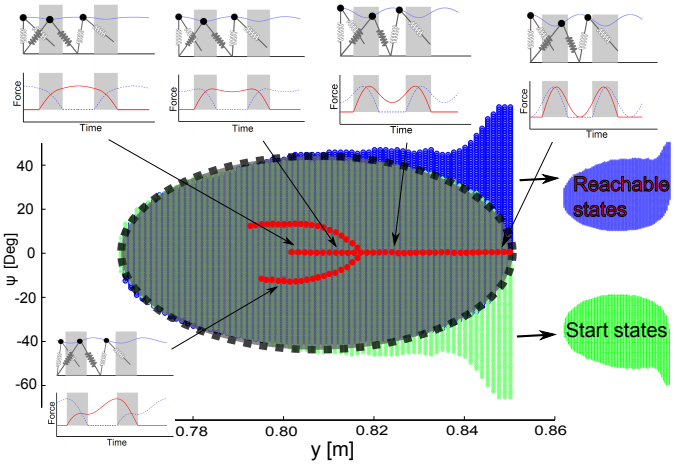

Fig. 2. Three regions are shown in the state space. The blue region shows the states that can be reached at the end of walking gaits. Green region shows the states that can start walking gaits and gray region (the elliptical region) is the workspace of the system which is the intersection of the reachable states and start states. The equilibrium points are highlighted with the red color. The behavior of the symmetric equilibrium gaits evolve from left to right as a continuous change. For those equilibrium gaits with small CoM height, the COM trajectory is like a straight line and as the CoM height increases at the Poincare section, the behavior of the system becomes bouncier until it evolves to hopping with two legs.

B. Workspace in different energy levels

Since the bipedal spring mass model is a conservative system, the workspace is defined assuming a constant system energy. However, on rough terrain, the changing level of the ground height changes the energy of the system, so we identify the workspace and the equilibrium gaits within it across a range of energy levels. The simulation example in section V shows the behavior of the system when it is disturbed by such a change in ground height.

IV. CONTROL POLICY

In this section, we introduce a deadbeat control policy for walking that vanishes the perturbations in the minimal number of steps.

Deadbeat control means a policy that exactly corrects the perturbation in a finite amount of time (usually minimal)

[25]. Mathematically, the return map f is called deadbeat on domain χ_d for a specific target X^* if there exists a $K \in \mathbb{N}$ such that [26]:

$$\overbrace{f \circ f \circ \cdots \circ f}^{K \text{ times}}(X) = X^* \quad \forall X \in \chi_d \tag{10}$$

The existence of the deadbeat control for running was shown for both 2D and 3D spring-mass models [25], [27]. In this section, we construct a deadbeat control policy for walking that pinpoints the target gait in the minimal number of steps.

As discussed in [25] using the implicit function theorem, a single step would be insufficient for stabilizing an equilibrium gait $(\boldsymbol{X^*}, \theta^*)$ in the bipedal spring-mass model. By varying the single control input θ from a given initial condition $\boldsymbol{X_n}$, the system can only reach a one-dimensional set of states $\boldsymbol{X_{n+1}}$ in the two dimensional $[y,\ \dot{y}]$ plane. Likewise, only a one-dimensional set χ_{d1} of states $\boldsymbol{X_n}$ can be mapped to $\boldsymbol{X^*}$ through the choice of θ_n (In figure 3, each blue curve shows the states that can reach each target equilibrium in red). For a hypothetical one-step controller, this deadbeat domain χ_{d1} has zero area; the single-step deadbeat control cannot be properly defined on a meaningful domain.

However, by increasing K to two steps, we can define a two dimensional subset χ_{d2} of the $[y,\ \dot{y}]$ plane as the region of attraction. For any X^*, χ_{d2} is the set of states $\boldsymbol{X_n}$ such that

$$A(\boldsymbol{X_n}, \theta_n) = \boldsymbol{X_{n+1}} \in \chi_{d1} \tag{11}$$

where

$$A(\boldsymbol{X_{n+1}} \in \chi_{d1}, \theta_{n+1}) = \boldsymbol{X^*} \tag{12}$$

for some sequential pair of touchdown angles θ_n and θ_{n+1}. Therefore, χ_{d2} is the set of states that can transition to some state in χ_{d1}, from which the target $\boldsymbol{X^*}$ can then be reached. This gives us the green regions in Figure 3. For any $\boldsymbol{X_n} \in \chi_{d2}$, we solve for θ_n numerically, having tabulated representations of state-to-state mapping A and intermediate domain $\chi_{d1}(\boldsymbol{X^*})$. In execution, we do not explicitly use θ_{n+1}, though if no disturbances are encountered after the first step, re-solving for θ_n at the next iteration yields the previous θ_{n+1} that satisfies $A(\boldsymbol{X_{n+1}}, \theta_{n+1}) = \boldsymbol{X^*}$. Thus, our feedback controller is expressed as

$$\theta_n = H(\boldsymbol{X_n}) = A^{-1}|_{\boldsymbol{X_n}}(\boldsymbol{X_{n+1}} \in \chi_{d1}), \tag{13}$$

where the existence of a valid intermediate state $\boldsymbol{X_{n+1}}$ is guaranteed by construction of domain χ_{d2}. This policy yields the Poincare map $f = A(\boldsymbol{X_n}, H(\boldsymbol{X_n})) : \chi \to \chi$ deadbeat stable on the two-dimensional subset χ_{d2}.

A. Properties and limitations of two-step control

By construction, $\boldsymbol{X^*} \in \chi_{d1} \subset \chi_{d2}$. The derived control gives the fastest possible convergence for any initial condition in χ_{d2}, and this region of attraction reflects the robustness of the stabilized gait. If the system is perturbed from the red point $\boldsymbol{X^*}$ to a state within this region, the limit cycle will be restored in two steps. Otherwise, more steps are required. Dynamic programming would naturally extend the formulation to optimally solve as many steps as desired (or sequential composition [28] as an approximate method), but here we implement $N = 2$ for sake of simplicity as it is the minimum for a domain of attraction with non-zero area.

Since χ_{d2} exactly represents the region of attraction of the two-step control, the size of χ_{d2} and the proximity of $\boldsymbol{X^*}$ to its boundaries measures the disturbances that the stabilized gait can handle. As can be seen in Figure 3, human-like two-humped walking gaits have large regions of attraction, and the nominal behaviors lie well within the boundaries. This shows that these gaits can handle relatively large disturbances in arbitrary directions.

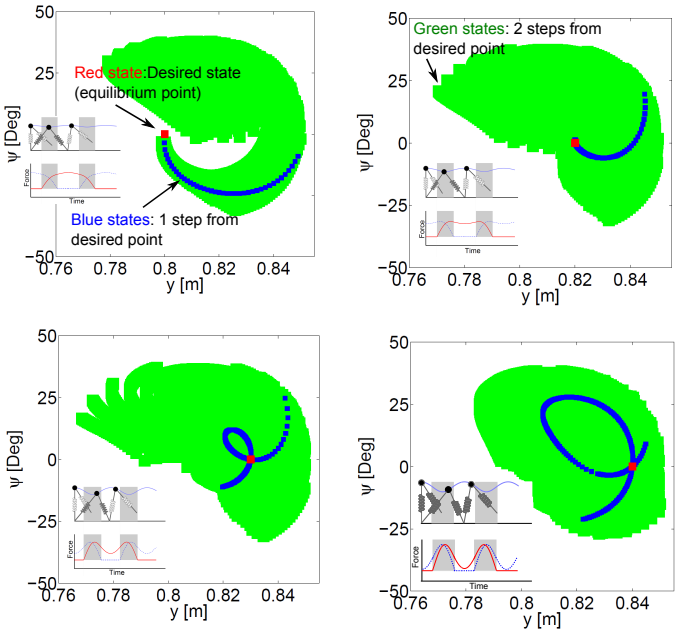

Fig. 3. Each of the figures above show the region (green area) in the workspace that can return to its equilibrium point (red point). The blue curve is the set of the states that can go to the equilibrium point in one step. When the equilibrium points (red points) are well inside the green region, they are less prone to disturbance. The leg force profile and the CoM trajectory of the red points are shown next to each part.

V. Simulation Results

In this section we show in simulation that the bipedal spring-mass model can accomplish the two-step deadbeat control and fully recover from random perturbations. Furthermore, we extend the policy from a constant energy level to different energy levels and show that the system can walk on rough terrain that the energy of the system changes due to the change of the ground level change.

We start by showing how to make transition from one equilibrium gait to another desired limit cycle using the two-step deadbeat control policy. In Figure 4, transition between the two equilibrium gaits is shown. The system starts from a limit cycle with Poincare state $A(y, \dot{y}) = (0.81m, 0^\circ)$ and goes to transition state $B(y, \dot{y}) = (0.817m, 12^\circ)$ and finally

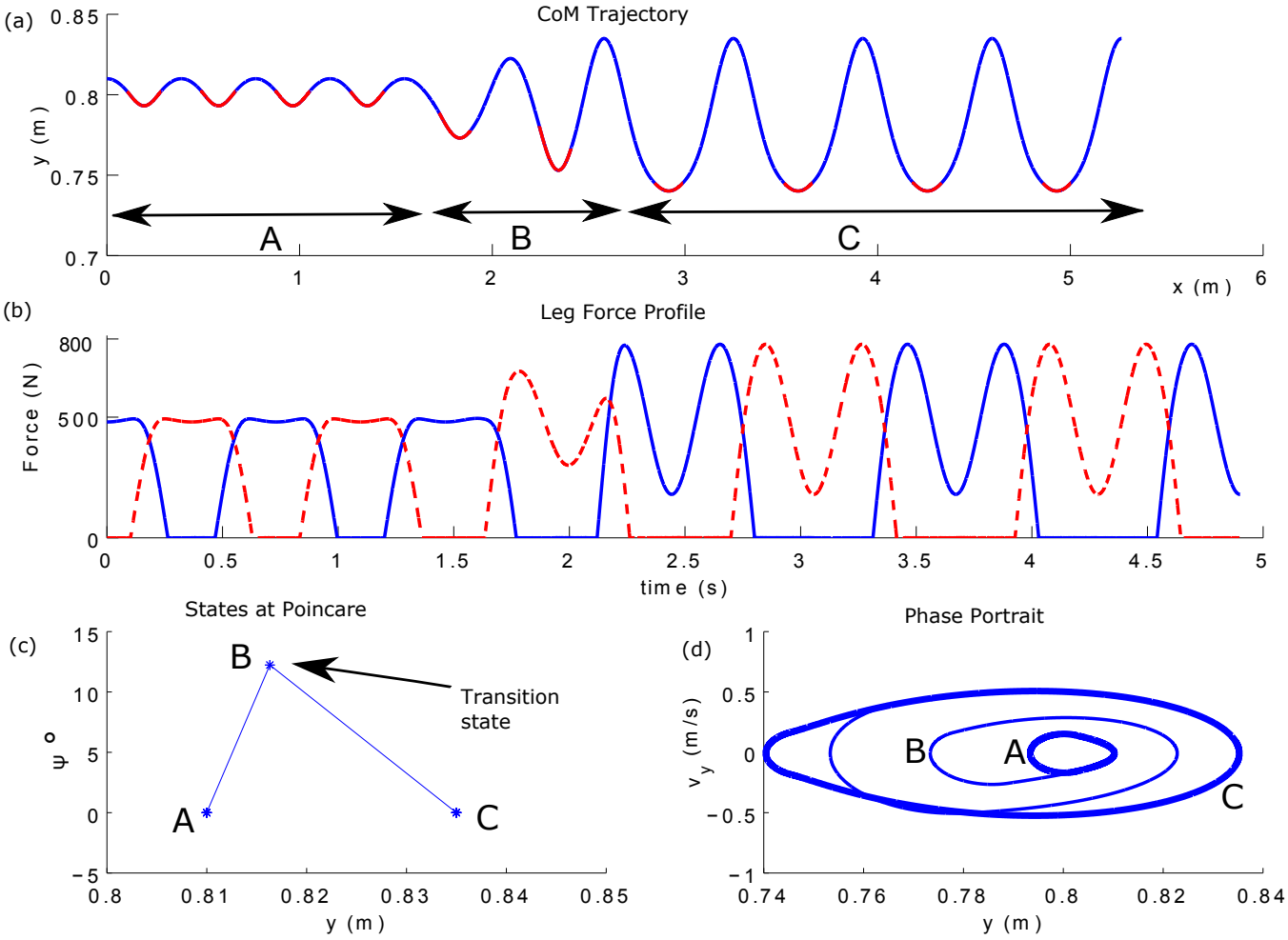

Fig. 4. Demonstration of the two-step deadbeat control policy for transitioning from $A(y, \psi) = (0.81m, 0°)$ to $C(y, \psi) = (0.835m, 0°)$ using $B(y, \psi) = (0.817m, 12°)$ as transition state. Part (a) shows the CoM trajectory of the system and in part (b) the leg force profiles are shown. The states at the Poincare section are demonstrated in part (c) and (d) shows the phase portrait of the system.

settles into $C(y, \psi) = (0.835m, 0°)$ using the deadbeat control policy.

Figure 5 shows the stability of the system under different perturbations. As it can be seen in the figure, various different initial conditions all converge to the desired gait $(y, \psi) = (0.83m, 0°)$ in two steps although the horizontal position and history of the CoM are different. The initial conditions are seen from the height and slope of the CoM trajectories $(y,\ \psi)$ at the beginning.

For walking on rough terrain, Figure 6 shows the model encountering an unexpected drop step with no prior information about the location and size of the disturbance. After the drop step, the preceding Poincare states as well as the system energy are changed. In the workspace of the new energy level, the two-step control to return to $\boldsymbol{X}^* = [y = 0.84m,\ \psi = 0°]$ is computed and applied. The drop step added energy to the system, so while $\boldsymbol{X}^*$ preserved its values of relative height y and direction of motion ψ across ground levels, the new equilibrium gait moves at a faster horizontal speed at the VLO. As can be seen, the new limit cycle is reached in exactly two steps.

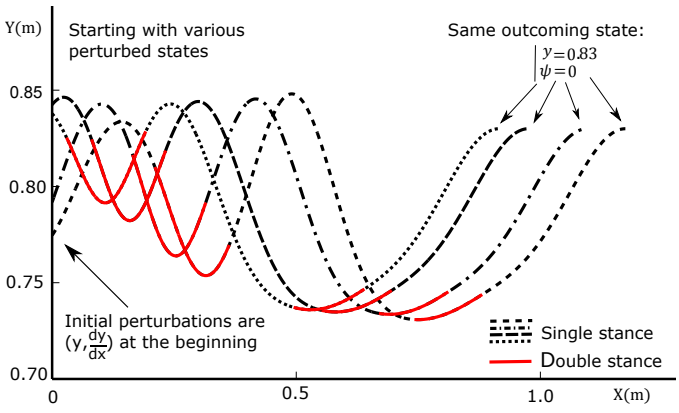

Fig. 5. Center of mass trajectory of the bipedal spring-mass model starting from various perturbed initial conditions. For all the cases, the system settles into the desired state in two steps. The double stance phases are shown in solid red lines and the dashed black lines are the single stance phases.

VI. Conclusions

In this paper we analyzed the dynamics of the bipedal spring-mass model and investigated the control authority

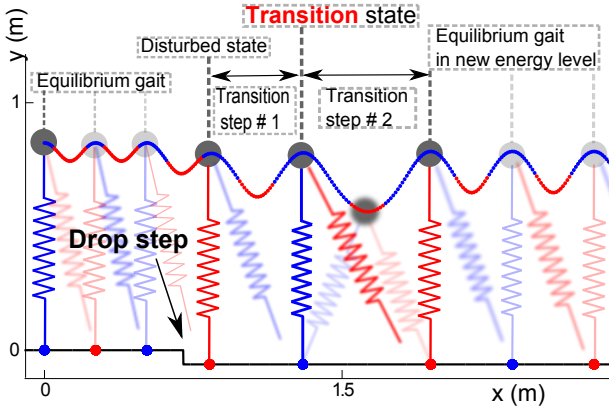

Fig. 6. Center of mass trajectory of the bipedal spring-mass model before and after a drop step in the ground. The system does not have prior information about the size and location of the disturbance. After the drop step, the system goes to a disturbed state in the new energy level (determined by the height of the drop step). To pinpoint the desired equilibrium gait, the system first goes to a transition state and after that it pinpoints the new desired equilibrium gait.

of the system for walking. We identified the periodic limit cycles and designed a deadbeat control policy to recover the system from perturbations in the fewest number of steps. We showed that at least two steps are necessary, and that two steps are sufficient to provide regions of attraction that cover significant portions of the workspace. The region of attraction of each stabilized limit cycle reflects its robustness, thus providing useful information for selecting robot walking gaits. We also observed that the gaits most similar to human-like walking have larger regions of attraction with the equilibrium point far away from the edges. Further, we extended the control to handle energy changes in the system from external disturbances like ground level changes and demonstrated its stability in simulation. To implement this control policy on the robot, look-up table for neighboring desired energy levels are required.

VII. Future Work

We intend to implement the control derived here for the simplified model on our SLIP-like robot ATRIAS [1]. ATRIAS is a spring-mass robot with the majority of the mass lumped at the hip to be as close as possible to the SLIP model.

Acknowledgment

This work is supported by the US National Science Foundation (CMMI-1100232).

References

[1] J. A. Grimes and J. Hurst. The design of atrias 1.0 a unique monopod, hopping robot. In *Proc 15th Int Conf on Climbing and Walking Robots (CLAWAR)*, 2012.

[2] J. A. Grimes, C. M. Hubicki, M. S. Jones, D. Renjewski, A. Sprowitz, and J. W. Hurst. Atrias 2.1: Enabling agile biped locomotion with a template-driven approach to robot design. *International Journal Robotic Research*, to be submitted, 2014.

[3] H. Geyer, A. Seyfarth, and R. Blickhan. Compliant leg behaviour explains basic dynamics of walking and running. *Proceedings of the Royal Society B*, 273:2861–2867, 2006.

[4] H. Geyer. *Simple models of legged locomotion based on compliant limb behavior*. PhD thesis, University of Jena, 2005.

[5] R. Blickhan. The spring-mass model for running and hopping. *Journal of Biomechanics*, 22:1217–1227., 1989.

[6] R. J. Full and D. E. Koditschek. Templates and anchors: Neuromechanical hypotheses of legged locomotion on land. *Journal of Experimental Biology*, 202:3325–3332., 1999.

[7] A. Seyfarth, H. Geyer, M. Guenther, and R. Blickhan. A movement criterion for running. *Journal of Biomechanics*, 35:649–655, 2002.

[8] P. Holmes, R. J. Full, D. Koditschek, and J. Guckenheimer. The dynamics of legged locomotion: Models, analyses, and challenges. *SIAM REVIEW*, 48:207–304, 2006.

[9] H. R. Vejdani, Y. Blum, M. A. Daley, and J. Hurst. Bio-inspired swing leg control for spring-mass running robots. *Bioinspiration & Biomimetics*, 8:046006, 2013.

[10] J. Rummel, Y. Blum, and A. Seyfarth. Robust and efficient walking with spring-like legs. *Bioinspiration & Biomimetics*, 5(4):046004, 2010.

[11] H. R. Martinez Salazar and J. P. Carbajal. Exploiting the passive dynamics of a compliant leg to develop gait transitions. *PHYSICAL REVIEW E*, 83:066707, 2011.

[12] I. Poulakakis and J. W. Grizzle. The spring loaded inverted pendulum as the hybrid zero dynamics of an asymmetric hopper. *Automatic Control, IEEE Transactions on*, 54(8):1779–1793, 2009.

[13] G. Garofalo, C. Ott, and A. Albu-Schaffer. Walking control of fully actuated robots based on the bipedal slip model. In *Robotics and Automation (ICRA), 2012 IEEE International Conference on*, pages 1456–1463, 2012.

[14] E. Andrada, C. Rode, and R. Blickhan. Grounded runningin quails: Simulations indicate benefits of observed fixed aperture angle between legs before touch-down. *Journal of Theoretical Biology*, 335:97–107, 2013.

[15] H. M. Maus and A. Seyfarth. Walking in circles: a modelling approach. *Journal of The Royal Society Interface*, 11(99), 2014.

[16] M. Garcia, Chatterjee A., Ruina A., and Coleman M. The simplest walking model: Stability, complexity, and scaling. *J Biomech Eng.*, 120:281–288, 1998.

[17] J. W. Grizzle, G. Abba, and F. Plestan. Asymptotically stable walking for biped robots: analysis via systems with impulse effects. *Automatic Control, IEEE Transactions on*, 46(1):51–64, 2001.

[18] K. Sreenath, H. W. Park, I. Poulakakis, and J. W. Grizzle. Compliant hybrid zero dynamics controller for achieving stable, efficient and fast bipedal walking on mabel. *The International Journal of Robotics Research*, 30:1170–1193, 2011.

[19] Fumiya Iida and Russ Tedrake. Minimalistic control of biped walking in rough terrain. *Autonomous Robots*, 28(3):355–368, 2010.

[20] R. D. Gregg, A. K. Tilton, S. Candido, T. Bretl, and M. W. Spong. Control and planning of 3-d dynamic walking with asymptotically stable gait primitives. *Robotics, IEEE Transactions on*, 28(6):1415–1423, 2012.

[21] E. R. Westervelt, J. W. Grizzle, C. Chevallereau, J. H. Choi, and B. Morris. *Feedback control of dynamic bipedal robot locomotion*. CRC press, Boca Raton, Florida., 2007.

[22] Hassan K. Khalil. *Nonlinear Systems*. Prentice Hall, 2002.

[23] J. Rummel, Y. Blum, H. M. Maus, C. Rode, and A. Seyfarth. Stable and robust walking with compliant legs. In *Robotics and Automation (ICRA), 2010 IEEE International Conference on*, pages 5250–5255, 2010.

[24] D. Schmitt. Insights into the evolution of human bipedalism from experimental studies of humans and other primates. *Journal of Experimental Biology*, 206:1437–1448, 2003.

[25] S. G. Carver, N. J. Cowan, and J. M. Guckenheimer. Lateral stability of the spring-mass hopper suggests a two-step control strategy for running. *Chaos*, 19:026106, 2009.

[26] Richard Altendorfer, Daniel E. Koditschek, and Philip Holmes. Stability analysis of a clock-driven rigid-body slip model for rhex. *International Journal Robotic Research*, 23(10-11):1001–1012, 2004.

[27] A. Wu and H. Geyer. The 3-d spring–mass model reveals a time-based deadbeat control for highly robust running and steering in uncertain environments. *IEEE Transactions on Robotics*, (99):1–11, 2013.

[28] R. R. Burridge, A. A. Rizzi, and D. E. Koditschek. Sequential composition of dynamically dexterous robot behaviors. *The International Journal of Robotics Research*, 18(6):534–555, 1999.